Available online at www.sciencedirect.com
SCIENCE DIRECT®
Journal of Power Sources 140 (2005) 181–202
JOURNAL OF POWER SOURCES
www.elsevier.com/locate/jpowsour

An algorithm for selection and design of hybrid power supplies for MEMS with a case study of a micro-gas chromatograph system

K.A. Cook[a], A.M. Sastry[a,b,*]

[a] *Department of Biomedical Engineering, University of Michigan, Ann Arbor, MI 48105, USA*
[b] *Department of Mechanical Engineering, University of Michigan, Ann Arbor, MI 48105, USA*

Received 20 May 2004; accepted 18 June 2004
Available online 2 December 2004

Abstract

The Wireless Integrated Microsystems (WIMS)-environmental monitor testbed (EMT) is a multi-component microelectromechanical system (MEMS), incorporating complementary metal oxide semiconductor (CMOS) materials for high-precision circuits used for integrated sensors such as micro-g accelerometers, micro-gyroscopes, and pressure sensors. The WIMS–EMT duty cycle, like many autonomous MEMS systems, has low-power standby periods for sensing, and high-power pulses for R/F transmission and reception. In this paper, we present results of three strategies for providing power to this system, including (1) specification of a single, aggregate power supply, resulting in a single battery electrochemistry and cell size; (2) specification of several power supplies, by a priori division of power sources by power range; and (3) specification of an arbitrary number of power "bundles," based on available space in the device. The second approach provided the best results of mass (0.032 kg) and volume (0.028 L) among the three approaches. The second and third approaches provided the best battery lifetime results; both systems produced lifetimes in excess of 2E3 h. Future work will incorporate CMOS operational amplifier (op-amp) technologies to accommodate large voltage fluxes in many MEMS devices, and implementation of our approaches into a user-friendly code.
© 2004 Elsevier B.V. All rights reserved.

Keywords: Microelectromechanical system; Micro-gas; WIMS–EMT

1. Introduction

The multicomponent Wireless Integrated Microsystems environmental monitor testbed (WIMS–EMT) is a microelectromechanical system (MEMS) whose goal is the realization of a wristwatch-sized device capable of sampling ambient pressure, temperature, humidity, and air quality [1]. The WIMS–EMT incorporates complementary metal oxide semiconductor (CMOS) materials for high-precision circuits used for integrated sensors such as micro-g accelerometers, micro-gyroscopes, and pressure sensors.

Supplying power to CMOS-based platforms has become increasingly challenging, due to nonlinear scaling of power consumption with respect to MEMS device size and mass, and difficulties associated with manufacture of thin-film batteries using CMOS fabrication techniques. CMOS devices are also prone to heat-induced failure [2–5]. Despite many advances in reduction in power consumption [2,6–8] of novel, higher-power and capacity micro and thin-film batteries [9–13] a cohesive methodology for design of power systems for MEMS has not, to our knowledge, been reported. Here, we introduce such an algorithm, which involves use of system constraints on operating temperature, storage battery life, energy/power density, specific energy/power; and battery characteristics, e.g. rechargeability, mass, volume, and lifetime. CMOS power consumption is a function of static and dynamic energy consumption, i.e.

$$P_{\text{total}} = P_{\text{SW}} + P_{\text{SC}} + P_{\text{static}} + P_{\text{leak}}. \quad (1)$$

Dynamic switching power, P_{SW}, is required to change charge to discharge functions. Short circuit power consump-

* Corresponding author. Tel.: +1 734 764 3061; fax: +1 734 647 3170.
E-mail address: amsastry@umich.edu (A.M. Sastry).

0378-7753/$ – see front matter © 2004 Elsevier B.V. All rights reserved.
doi:10.1016/j.jpowsour.2004.06.071

tion, P_{SC}, results from current traveling between the power supply and ground during gate switching. The static power component, P_{static}, results from other factors, including bias current. Finally, power consumption due to leakage current, P_{leak} results from gate-oxide tunneling current, source to drain sub-threshold conduction, and *pn*-junction leakage [14]. Of these, the dominant component of power consumption in CMOS devices is dynamic switching power (85–90%) [2], and a first order approximation of this term can be expressed as:

$$P_{SW} = \alpha \chi V_{supply}^2 f \quad (2)$$

where χ is capacitance due to charge/discharge switching, α is an activity-weighting factor that represents the probability that a transition occurs, V_{supply} is the supply voltage, and f is the frequency of operation. Many workers have focused on reducing the factors that most influence dynamic power consumption, namely capacitive load, supply voltage, switching frequency, and activity (e.g. [2,6–8]). However, alteration of some of these parameters can independently reduce performance; for example, reduction in supply voltage generally results in slower speed of execution of instruction sets a processor can execute, bandwidth, and clock speed.

Reductions in dynamic power have been forecasted, with reductions in scale of CMOS technology to deep-submicron levels. MOS transistor channel lengths have been produced with dimensions under 100 nm, and device gate-oxide isolation have been reported of less than 2 nm. Thus, power due to component leakage is predicted to ultimately surpass dynamic power [2]. The ITRS-2001 (International Technology Roadmap for Semiconductors in 2001), has predicted that operating voltage will decrease from 1.2 V (2001) to 0.5 V (2013), and that the maximum number of transistors per chip of most silicon technologies will increase from 7 million (2001) to 8 billion (2013) due to circuit device techniques such as multi-threshold CMOS [15], adaptive reverse body biasing [16], and microarchitectural and compiler techniques. For example, wireless personal area communication devices (CD), high-end user interface devices (also called master devices, MD), and low-end user devices are projected to require active power supplies in the ranges of 100, 10, and 1 mW, respectively, and standby power consumption values of 10 mW, 1 mW, and 100 μW, respectively [2,3]. Switching power consumption in these devices (using values from ITRS-2001—International Technology Roadmap for Semiconductors in 2001), are predicted to decrease from ∼300 mW in 2004, to less than 1 mW by 2013; while static power is predicted to increase from 0.25 W in 2004 to 4.25 W by 2013 [2,3]. Scaling of large devices via implementation of CMOS technology will remain nonlinear with respect to reduction in power supply.

Specific energy and power (with typical dimensions $Wh\,kg^{-1}$ and $W\,kg^{-1}$, respectively) and energy and power densities (with typical dimensions $Wh\,L^{-1}$ and $W\,L^{-1}$, respectively) are generally used to characterize the mass and volumetric efficiency of a power supply [17], though these values alone are insufficient to prescribe a system. Because many secondary batteries exhibit capacity fade and rate-dependence, along with temperature and other environmental constraints, more information is needed to select an appropriate power supply.

Thin-film electrochemistries have been developed, of sizes ranging from 1 to 21.7 cm^2 in surface area, 8 μm and 3.6 mm in thickness, with current discharge rates, voltages, and specific energy ranging from 0.1 to 1.6 C, 1.5–4.0 V, and 26.3–350 ($Wh\,kg^{-1}$), respectively, listed in Table 1 (per reported values in [9,10,12,13]). However, implementation of these batteries into "real-world" devices has been problematic, since CMOS fabrication temperatures routinely exceed 250 °C, which is above the boiling point of some battery materials (e.g. lithium metal, at 180.5 °C) [18]. Tin oxide can be processed and cycled at high temperatures [18]. However, it cannot provide the same capacity as lithium metal, and is thus often an unsuitable replacement.

Factors influencing selection of power supply can be summarized as follows:

(1) *electrochemistry*: cell potential, discharge/charge profile, capacity, and lifetime
Conductivity of active materials largely determines the maximum cell discharge/charge rates, and cell capacity. For example, Bates et al. [9] compared the performance of thin-film lithium metal rechargeable batteries which used an amorphous inorganic electrolyte, amorphous V_2O_5 and $Li_xMn_2O_4$ as cathode materials. They found that the performance of rechargeable thin-film lithium batteries depended critically on methods used to deposit the cathodes, their geometry, operating temperature, and current density.
(2) *geometry*: surface area, volume, and mass
Cells designed for long service life, or high capacity at low to moderate discharge currents, require commensurately high volumes of active material. Those designed for high discharge rates often have lower total volume of active material, but high surface areas. For example, the spirally wound, Duracell, CR2, lithium manganese cell, has a mass of 11 g, volume of 5.168 cm^3, and capacity of 0.5 Ah at 1 A discharge current, which has superior higher rate performance over its bobbin construction counterpart—the Duracell MX1500-AA [19].
(3) *environment*: temperature, pressure, and exposure
Sufficiently low-operating temperatures result in reduced capacity, and increase the negative slope of the voltage curve due to decreased chemical activity, and enhanced internal resistance. However, high-operating temperatures can result in self-discharge [20]. For example, Liaw et al. [20] found for cylindrical 18650 lithium-ion cells, increasing temperature produced greater capacity and power fade. However, as the state of charge decreased, the amount of power fade expressed at each temperature decreased relative to the 100% state of charge.

Table 1
Thin-film battery technologies [9,10,12,13]

Electrochemistry	Dimensions	Volt	Specific energy (Wh kg^{-1})	Energy density (Wh L^{-1})
Solid state, thin-film cathode = V_2O_5, electrolyte = block polymer, anode = lithium [13]	Area = 1 cm^2, thickness = 20 μm	1.5–4.0	350 @1.6 C	560 W kg^{-1} @1.6 C
Thin-film, cathode = $LiCoO_2$, anode = MCF (mesophase-pitch-based carbon fiber), electrolyte = organic liquid [12]	Area = 21.7 cm^2, thickness = 1.2 mm	∼3.8 V	120 @0.2 C	–
Thin-film, cathode = $LiCoO_2$, anode = MCF (mesophase-pitch-based carbon fiber), electrolyte = organic liquid [12]	Area = 21.7 cm^2, thickness = 3.6 mm	∼3.8 V	160 @0.2 C	–
Thin-film, cathode = $LiCoO_2$, anode = B-doped MCF (mesophase-pitch-based carbon fiber), electrolyte = organic liquid [12]	Area = 21.7 cm^2, thickness = 1.2 mm	∼3.8 V	172 @0.2 C	–
Thin-film, solid state, cathode = TiS_2, anode = lithium, electrolyte = oxide/sulfide glassy [10]	Thickness = ∼10 μm	∼2.4–2.5 V	140 Wh L^{-1} @135 mA cm^{-2}	270 W L^{-1}
Thin-film rechargeable lithium, cathode = V_2O_5, anode = lithium metal, electrolyte = amorphous inorganic electrolyte [9]	Area = 6.25 cm^2, cathode thickness = 0.13 μm, electrolyte thickness = 1 μm, lithium thickness = 3–5 μm	1.5–3.5	26.3 @.13 C	14.4 @0.13 C
Thin-film rechargeable solid state, cathode = TiS_2, anode = lithium metal, electrolyte = oxide/sulfide glassy electrolyte [10]	Thickness = 10 μm	1.8–2.5 V	–	140 @ 75–135 μA cm^{-2}

Often, two or more power supplies are used within the same system to overcome some of the limitations of electrochemistry, size, shape, and conditions outlined above. The WIMS–EMT, like many autonomous MEMS systems, has low-power standby periods for sensing, and high-power pulses for R/F transmission and reception [24]. Typically, a hybrid power supply combines a high-power density/low-energy density power element to support high pulses, and high-energy density/low-power density element to provide low, sustained power [21]. Such systems have been designed, for example, for automotive applications (e.g. polymer electrolyte membrane (PEMFC) fuel cell/lead-acid battery studied in [22]), and civilian power systems (e.g. the wind/diesel/battery system studied in [23]). These studies, among others, have shown that improved performance is possible with hybrid supplies, though the power supplies in the cases mentioned were pre-selected.

2. WIMS–EMT: requirements

The WIMS–EMT consists of a micro-gas chromatographic (micro-GC) system and MEMS control circuitry designed for separation and analysis of volatile compounds in the environment [1]. Like many "wireless devices" presently under development, the WIMS–EMT uses radio waves instead of current-delivering wires, to transmit signals. The micro-GC contains two gas chromatographic columns for sample separation, one heated preconcentrator for collection and concentration of volatile gaseous compounds, a micropump and several valves used to cycle the gases through the system, a thermal electric cooler to cool the sensor array, and a sensor array for the detection and analysis of volatile compounds in the air. The MEMS control circuitry contains a micro-control unit (MCU), a Universal Micro-Sensor Interface (UMSI) chip, and a radio frequency evaluation board, all of which operate according to the generic multi-element MEMS architecture, established as a platform for low-power wireless applications where small size and sensing accuracy are vital [24].

The power consumption in the device spans the watt 3.7 W to microwatt 200 μW ranges (with component power requirements listed in Table 2). The targets for power system volume and mass are, respectively, 1.45 cm^3 and 0.0043 kg; the total system volume is ∼65.08 cm^3. The maximum and minimum (aggregate) power requirements for the WIMS–EMT are ∼4.65 and 1.125 W, respectively; maximum and minimum (aggregate) discharge currents are ∼0.512 and 0.327 A.

The goals of this paper are to describe a systematic method for the selection and design of power systems for MEMS devices, wherein a case study of the WIMS–ERC will be performed. The three strategies are:

Table 2
WIMS–EMT component list of voltage and power requirements

Component	Power (mW)	Voltage (V)
Chromatographic columns one and two	450	15
Sensor array	0.20	3
Thermal cooler	200	3
Microvalves	100	1.5
Vacuum pump	780	6
MCU	Sustained = 10	0.9
(40 MHz)	Peak = 22	1.8
Ambient sensors	Negligible	3
UMSI chip	12	3
Preconcentrator	Sustained = 650	3.0
	Peak = 3700	16.64
RF evaluation board	Sustained = 45	3
	Peak = 125	

- specification of a single, aggregate power supply, resulting in a single battery electrochemistry and cell size;
- specification of several power supplies, by a priori division of power sources by power range, e.g. the μW, mW, and W used in the testbed, resulting in a hybrid power system with a maximum (here) of three electrochemistry types and cell geometries; and
- specification of an arbitrary number of power "bundles," based on available space in the device, yielding either a homogenous or hybrid power system with one or more types of electrochemistry and cell geometries.

3. Methods

A general overview of the algorithm is shown in Fig. 1. Final power configurations consist of electrochemical cells arranged in series or parallel. Resistors, operational amplifiers (op-amps), and capacitors are routinely used to obtain higher voltage values or modify current discharge values in

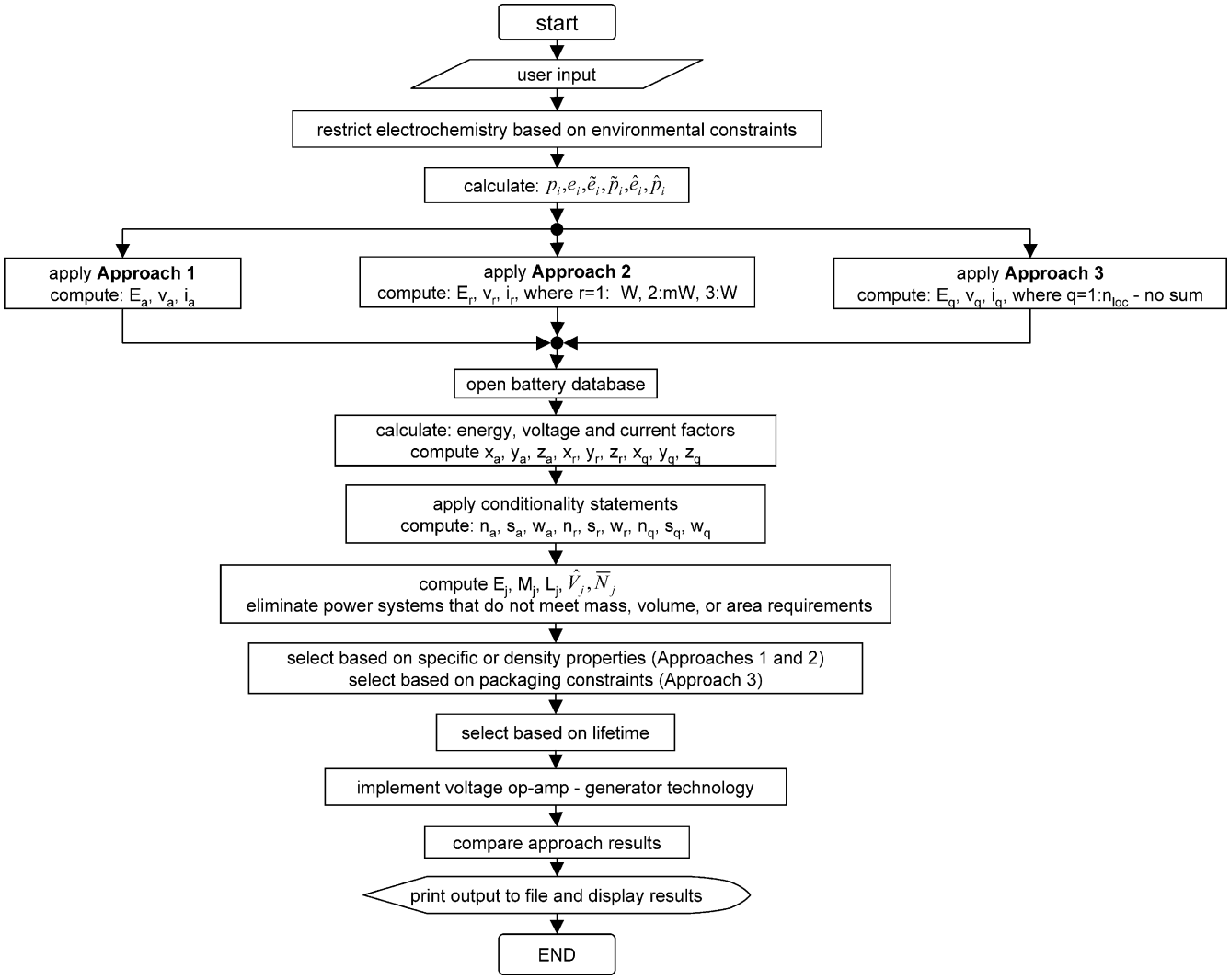

Fig. 1. Overview of the power selection algorithm.

these applications. Other workers have used CMOS op-amps [25,26], to alter the supply voltage for MEMS devices. After selection of batteries, we used specifications of a set of three commercially-available op-amps and one voltage generator to reduce the number of batteries required only to drive up voltage.

A stepwise outline of the algorithm follows:

1. User supplies power system targets (mass, volume, area, etc.) and subdevice requirements (current and voltage) and environmental constraints.
2. Environmental requirements are used to eliminate electrochemistries.
3. Subdevice performance parameters are computed (power, specific energy and power, and energy and power densities).
4. Approaches 1, 2, and 3 are applied to subdevice parameters.
5. Energy, voltage, and current ratios (maximum/available from cell) are computed for each battery in the reduced database.
6. Conditionality statements are applied to compute the total numbers and required arrangements of battery.
7. Power configurations are eliminated based on mass, volume, or area target values. If no batteries meet these targets, a maximum of three batteries that have values closest to target values are selected.
8. Batteries are selected based on specific or energy properties for Approaches 1 and 2, and based on packaging constraints for Approach 3.
9. Batteries are selected based on maximum lifetime.
10. Results from all three approaches are compared and one system is selected.

We note that system cost was not used as a criterion in the inherently high-cost, high-tech application studied here, though this would clearly be a first-order concern in consumer electronics. The second approach studied here was limited to evaluation of power ranges of μW, mW, and W used in the testbed for definiteness, though extension to other ranges would be straightforward.

3.1. User input and calculation of device parameters

A list of required input data is provided as Table 3. The algorithm developed here assumed user-provided power constraints, including power system mass, m_{sys}; volume, v_{sys}; areal footprint, a_{sys}; maximum number of power bundles, n_{loc}; mass range values, m_1, m_2, and m_3 (subscripts 1 = μW, 2 = mW, and 3 = W); and volume range values, v_1, v_2, and v_3; and mass, volume, and area bundle values $\underline{m}_q$, $\underline{v}_q$, and $\underline{a}_q$, respectively, where $q = 1{:}n_{loc}$. Also provided were the number of subdevices, N; and discharge current ($c_j(t)$) and voltage values ($v_j(t)$), where $i = 1{:}N$, for each time interval of a cycle; battery selection priority (mass or volume); type of battery (primary or secondary); and environmental constraints (discharge and charge temperature, pressure, and magnetic material limitations).

Table 3
Input parameters supplied by the user, associated variable names, and data type

Input parameters	Name	Type
Number of devices	N	Integer
Current vs. time for each device	$c_j(t)$ $j{:}1 = N$	Real number
Voltage vs. time for each device	$v_j(t)$ $j{:}1 = N$	Real number
Ambient temperature (K)	T	Real number
Use of primary or secondary devices	<p> or <s>	Single string character
Volume or mass optimization	<v> or <m>	Single string character
Desired mass for power supply (kg)	m_{sys}	Real number
Desired volume for power supply (cm^3)	v_{sys}	Real number
Maximum surface area for power supply (cm^2)	a_{sys}	Real number
Number of operation cycles	n_{cyc}	Integer
Maximum number of power bundles	n_{loc}	Integer
Mass μW power range	m_1	Real number
Mass mW power range	m_2	Real number
Mass W power range	m_3	Real number
Volume μW power range	v_1	Real number
Volume mW power range	v_2	Real number
Volume W power range	v_3	Real number
Bundle 1 area	$\underline{a}_1$	Real number
Bundle 2 volume	$\underline{v}_2$	Real number

Power requirements per time increment are computed from the parameters of Table 3. Power, $p_i(t)$, is simply the product of voltage $v_i(t)$ (V) and current, $c_i(t)$ (A), per

$$p_i(t) = c_i(t)v_i(t), \quad i = 1 : N, \text{ no sum} \tag{3}$$

Energy, e_i, is the product of power and time increment, given by:

$$e_i = p_i(t)\Delta t \tag{4}$$

specific energy, $\tilde{e}_i$, is energy per unit mass,

$$\tilde{e}_i = \frac{\Delta t p_i(t)}{m_x} \tag{5}$$

weighted specific power, $\tilde{p}_i$, is power per unit mass,

$$\tilde{p}_i = \frac{(\Delta t/t_T)p_i(t)}{m_x} \tag{6}$$

energy density, $\hat{e}_i$, is energy per unit volume given by:

$$\hat{e}_i = \frac{\Delta t_i p_i(t)}{v_x} \tag{7}$$

and weighted power density, $\hat{p}_i$, is power per unit volume,

$$\hat{p}_i = \frac{(\Delta t/t_T)p_i(t)}{v_x}. \tag{8}$$

In the previous expressions t_T (s) is the duration of a single cycle. Subscript $x = a$, corresponds to the aggregate system

parameters. For $x = r$, subscript r takes values of 1 for the microwatt (μW) power range, 2 for the milliwatt (mW) power range, and 3 for the watt (W) power range. For $x = q$, we have values of q from 1:n_{loc}, corresponding to the number of power bundle locations. Eqs. (4)–(8) are evaluated independently for Approaches 1, 2, and 3, respectively.

3.2. Restriction of electrochemistry based on environmental constraints

The batteries evaluated by the algorithm were selected from a database comprising 25 commercial secondary (rechargeable) batteries, representing the following electrochemistries: manganese lithium, nickel metal hydride, lithium-ion, and nickel cadmium. One type of thin-film battery (lithium-free) was included [27] for application to Approaches 2 and 3. These commercially available battery electrochemistries were selected due to their relatively low masses (∼4.5–73 g) and volumes (∼0.03–56.50 cm^3), making them generally suitable for MEMS applications. The battery database developed for this work includes performance characteristics, such as mass, volume, capacity (at a defined discharge rate (C)), nominal discharge/charge current, and nominal voltage, per Table 4.

3.3. Application of Approaches 1, 2, and 3

Approach 1 requires the summation of device values for power, $p_i(t)$ over each time increment to produce an aggregate device power versus time profile. The aggregate power data for the system was used to compute aggregate system parameters such as energy, E_a and weighted power, P_a, from Eqs. (9) and (10) as:

$$E_x = \sum_{j=1}^{N} p_j(t)t \tag{9}$$

and

$$P_x(t) = \sum_{j=1}^{N} p_j(t)\frac{t}{t_T} \tag{10}$$

where subscript x is a for aggregate system of device parameters; r for each power range ($r = 1$, 2, and 3 for μW, mW, and W power ranges, respectively).

In Approach 2, device power values are separated according to power range: microwatt, milliwatt, and watt, wherein the power and current data were summed over each time increment within each power range. This logic was performed in iterations: subdevices contributing to the largest power values within a particular power range were removed and placed in a higher power range than their initial position as needed. Once both guidelines for the micro and milliwatt power ranges are met, final power versus time profiles for each power range were assembled so that energy, E_1, E_2, and E_3; weighted power, P_1, P_2, and P_3 could be calculated from Eqs. (9) and (10).

In Approach 3, user-defined values included the number of available power bundle locations, wherein grouping is based on availability of space and surface area; the volumes, surface areas, and mass target values were also collected. The required energy for each site location is computed based on the fraction of total space required for a particular bundle. For example, if three locations have volume and areal footprint requirements of $\underline{v}_1 = 2.5\,cm^3$, $\underline{v}_2 = 3.5\,cm^3$, $\underline{v}_3 = 5\,cm^3$, $\underline{a}_1 = 1.0\,cm^2$, $\underline{a}_2 = 0.5\,cm^2$, and $\underline{a}_3 = 0.75\,cm^2$, respectively; then the fraction of energy required for each location is computed as:

$$\alpha_q = \frac{\underline{v}_q}{\sum_{q=1}^{n_{loc}} \underline{v}_q} \tag{11}$$

where the energy for each location is given as:

$$E_q = \alpha_q E_a \tag{12}$$

where E_a is computed from Eq. (9). The weighted power is computed in a similar manner, wherein a fraction of the surface areas is given by:

$$\beta_q = \frac{\underline{a}_q}{\sum_{q=1}^{n_{loc}} \underline{a}_q} \tag{13}$$

and the weighted power is given by:

$$P_q = \beta_q P_a. \tag{14}$$

After power versus time profiles have been constructed for Approaches 1 and 2, and the energy and weighted power have been computed for Approach 3, we obtain specific energy for Approaches 1 and 2 as:

$$\tilde{E}_x = \sum_{i=1}^{N} \tilde{e}_i \tag{15}$$

weighted specific power given by:

$$\tilde{P}_x = \sum_{i=1}^{N} \tilde{p}_i \tag{16}$$

energy density given by:

$$\hat{E}_x = \sum_{i=1}^{N} \hat{e}_i \tag{17}$$

and weighted power density given by:

$$\hat{P}_x = \sum_{i=1}^{N} \hat{p}_i \tag{18}$$

by summing device values per time increment. The specific and energy values for Approach 3 are determined by multiplying the specific energy and energy density values computed for Approach 1 by α_q for each bundle site. Similarly, the specific power and power density values for Approach 3 can be calculated by multiplying the values from Approach 1 by β_q.

Table 4
Database of commercial batteries

Manufacturer	Anode - Cathode	Battery Shape	Part Number	Height (mm)	Width (mm)	Length (mm)	Diameter (mm)	Area (cm^2)	Volume (cm^3)	Mass (g)	Discharge Current (mA)	Resistance (Ω)	Capacity (mAh)	Nominal Voltage (V)	Cut-Off Voltage (V)	Number of Cycles	Specific Energy (Wh/kg)	Energy Density (Wh/L)
Panasonic	Lithium - Manganese Dioxide	coin	ML414S	1.4	-	-	4.8	0.18	0.03	0.08	0.005	600000	1.20	3	2	1000	45.00	142.10
			ML421S	2.1			4.8	0.18	0.04	0.11	0.003	1000000	2.30	3	2	1000	62.73	181.58
Panasonic	AB_5 type alloys - Nickel Hydroxide	spirally wound cylindrical	HHR60AAAH	44.5	-	-	10.5	0.87	3.85	12.00	100	30.00	500	1.2	1	500	50.00	155.71
			HHR70AAAJ	44.5			10.5	0.87	3.85	13.00	144	20.83	720	1.2	1	500	66.46	224.23
Energizer			NH50-D	61.50	-	-	34.20	9.19	56.50	73	500.00	2200.00	2500	1.2	1.00	500	41.10	53.10
			NH35-C	50.00	-	-	26.20	5.39	26.96	60	500.00	2200.00	2500	1.2	1.00	500	50.00	111.29
			NH12-AAA	44.50	-	-	10.50	0.87	3.85	12	170.00	750.00	850	1.2	1.00	500	85.00	264.71
			NH15-AA	50.50	-	-	14.50	1.65	8.34	27	460.00	1850.00	2300	1.2	1.00	500	102.22	330.97
			NH22-9V	16.90	26.50	48.50	-	12.85	21.72	41	30.00	1500.00	150	1.2	1.00	500	4.39	8.29
Supreme Technologies			SP75AAAMH	42.5	-	-	10	0.79	3.34	13	150.00	8.00	750	1.2	0.9	500	69.23	269.63
			SP180AAKH	50	-	-	14.2	1.58	7.92	28	360.00	3.33	1800	1.2	0.9	500	77.14	272.78
			SP230AAKH	50	-	-	14	1.54	7.70	30	460.00	2.61	2300	1.2	0.9	1000	92.00	358.59
Panasonic	Crystallized Carbon - Lithium Cobalt Oxide	spirally wound cylindrical	CGR17500	49.6	-	-	16.9	2.24	11.13	25	156	19.23	830	3.6	3	500	119.52	268.56
			CGR18650HG	65.0	-	-	18.5	2.69	17.47	42	340	8.82	1800	3.6	3	500	154.29	370.88
Maxell	Crystalized Carbon - Lithium Cobalt Oxide	prismatic flat plate	ICP063047G	6.6	30.3	47.3	-	14.33	9.46	20	180	20.56	900	3.7	2.75	500	166.50	352.04
			ICP053048G	5.60	29.80	48.00	-	14.30	8.01	17.00	156	23.72	780	3.70	2.75	500	169.76	360.29
			ICP063450G	6.50	34.00	49.60	-	16.86	10.96	23.00	220	16.82	1100.00	3.70	2.75	500	176.96	371.30
			ICP383450G	3.90	34.00	49.70	-	16.90	6.59	14.50	140	26.43	700	3.70	2.75	500	178.62	393.01
			ICP043048G	4.60	29.50	47.80	-	14.10	6.49	14.50	144	25.69	720	3.70	2.75	500	183.72	410.70
Panasonic	Crystalized Carbon - Lithium Cobalt Oxide	prismatic flat plate	CGA523450A	5.25	34	50		17.00	8.93	19.5	900	3.33	910	3.6	3	500	168.00	367.06
			CGA523436	5.2	34	36	-	12.24	6.36	14.5	680	4.41	700	3.6	3	500	173.79	395.93
Panasonic	Metal Cadmium - Nickel Oxyhydroxide	spirally wound cylindrical	P-11AAH	17.50	-	-	14.50	1.65	2.89	6.5	24.000	50.000	120	1.2	1	500	22.15	49.83
			P-18N	30.00	-	-	12.00	1.13	3.39	8	38.000	31.579	190	1.2	1	500	28.50	67.20
Supreme Technologies	Metal Cadmium - Nickel Oxyhydroxide	spirally wound cylindrical	SP30AA2/3MC	28.5	-	-	14.2	1.58	4.51	11	1500.00	0.800	300	1.2	1	500	32.73	79.76
			SP28AAAMC	42.4	-	-	10.2	0.82	3.46	9	1400.00	0.857	280	1.2	1	500	37.33	96.98
-	Copper - Lithium Cobalt Oxide	thin film	-	Thickness: 1500 Angstrom Cu anode current collector/ 2μm Lipon electrolyte/ 1.6 μm $LiCoO_2$ cathode				1.00	-	-	0.10	42000	0.72	4.2	3	1000	energy density = 0.001 Wh/cm^2	

3.4. Calculation of energy, voltage, and current factors

Within a power system, total system energy,

$$e_j = \sum_{i=1}^{t_T} b_j C_j \frac{t}{t_T} \tag{19}$$

is based on placement of batteries; series placement achieves higher voltage, and parallel placement achieves higher discharge current. In Eq. (19), b_j is the nominal voltage, with $j = 1{:}d$, and where d is the number of batteries selected from the database. C_j, is the cell capacity, at time, t; t_T is the time interval. Energy values for each approach, were calculated for the aggregate system, power ranges, and bundle sites using Eq. (9).

Cell energy, e_j, nominal voltage, b_j, and maximum allowable discharge current, i_j, are related to system, power range, or power bundle values for energy (E_a, E_r, E_q), maximum voltage (V_a, V_r, V_q), and maximum discharge current (i_a, i_r, i_q) via:

$$x_j = \frac{E_x}{e_j} \tag{20}$$

$$y_j = \frac{V_x}{b_j} \tag{21}$$

and

$$z_j = \frac{i_x}{i_j}. \tag{22}$$

All factors computed from Eqs. (20)–(22) are first rounded up to the nearest integer, and then substituted into conditional statements.

3.5. Apply conditionality statements

Conditional statements are used to determine the number of batteries and cell configuration required, i.e. placement of batteries in series, parallel, and/or a combination required for system operation. Conditional statements have been derived for each possible combination of x, y, and z along with corresponding circuit diagrams illustrated in Table 5(a) and (b) , where n_a, n_r, and n_q are the total number of batteries; s_a, s_r, and s_q are the total number of batteries in series; and w_a, w_r, and w_q are the total number of batteries in parallel for Approaches 1, 2, and 3, respectively. For conditions specified in Table 5(a), the total number of batteries in the system is:

$$n_j = y_j z_j \tag{23}$$

the number of batteries which must be placed in series is:

$$s_j = y_j \tag{24}$$

and the number of batteries which must be placed in parallel is:

$$w_j = z_j. \tag{25}$$

For conditions specified in Table 5(b), total number of batteries is:

$$n_j = y_j z_j + |x_j - z_j| \tag{26}$$

where the number of batteries in series is found using Eq. (24), and the number of batteries in parallel to meet the discharge current requirement is given by:

$$w_j = y_j - z_j \tag{27}$$

The number of parallel-placed batteries required in to meet the energy requirement is then given by:

$$u_j = x_j. \tag{28}$$

When factor x is less than or equal to 1 the energy provided from a single cell can supply enough energy for one cycle of operation. If x is greater than 1, cells must be placed in parallel to meet the energy requirements while maintaining operation at a specific voltage value. For example, if $x = 3$, then three batteries placed in parallel will satisfy the energy requirement, as illustrated in Fig. 2. Also, if z is less than or equal to 1, the required discharge current for the application can be met with one cell, however, if this value is greater than 1, additional cells placed in parallel are necessary. Placing the cells in parallel, allows the current draw to be divided amongst the cells to prevent cell malfunction due to overly high discharge rates. Hence, if $z = 3$, Fig. 2 is also appropriate. If y is less than or equal to 1, then only 1 cell is required to satisfy the voltage requirements. However, if y is greater than 1, cells must be placed in series. For example, if $y = 3$, then three cells are required, as depicted in Fig. 2. In systems containing many subdevices, various combinations of x, y, and z can be used to satisfy the application.

3.6. Elimination based on mass, volume, or area targets

The total amount of energy provided by the system of cells given by:

$$E_j = e_j n_x. \tag{29}$$

Total mass and volume, are, respectively,

$$M_j = m_j n_x \tag{30}$$

and

$$\hat{V}_j = \hat{v}_j n_x. \tag{31}$$

For example: for a system requiring $E_a = 0.1$ Wh, $i_a = 0.1$ mA, $v_a = 3.0$ V and for which two batteries are examined (Lithium, CR927-Renata, with $E_1 = 0.09$ Wh, $i_1 = 0.05$E-3, $v_1 = 3.0$ V; and NiMH, HHR60AAAH, Panasonic, with $E_2 = 0.6$ Wh, $i_2 = 0.11$ A, $v_2 = 1.2$ V) we can calculate the total number of required batteries as 2 and 3, respectively. The number of cycles a battery system can provide is simply given by:

$$\bar{N}_j = \frac{E_j}{E_x}. \tag{32}$$

Table 5
(a) Conditionality statements applicable to cases where y or z has the maximum value of the three factors; (b) conditionality statements applicable to cases where x has the maximum value of the three factors, or where x is greater than z

Condition	Expression	Examples and circuit diagram	x	y	z	n_j	s_j	w_j
(a)								
$x = y = z$			1	1	1	1	1	1
		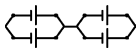	2	2	2	4	2	2
		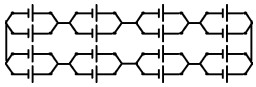	4	4	4	16	4	4
$x < y < z$	$n_j = yz$, $s_j = y$, $w_j = z$	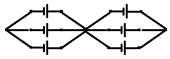	1	2	3	6	2	3
		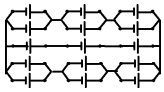	2	3	5	15	3	5
$y < x < z$			2	1	3	3	1	3
		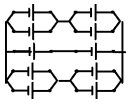	3	2	5	10	2	5
$x < z < y$		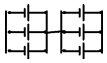	1	3	2	6	3	2
		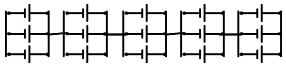	2	2	6	15	5	3
$x = y < z$			1	1	2	2	1	2
		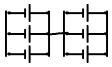	2	2	3	6	2	3
$x = z < y$			1	2	1	2	1	2
		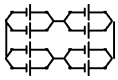	2	4	2	8	4	2
$x = z > y$			2	1	2	2	1	2
		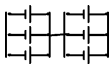	3	2	3	6	2	3
$y = z > x$		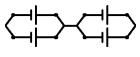	1	2	2	4	2	2
		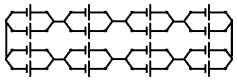	2	4	4	16	4	4

Table 5 (*Continued*)

Condition	Expression	Examples and circuit diagram	x	y	z	n_j	s_i	w_j and u_j
(b)								
$z < x < y$			2	3	1	4	3	1 and 2
			3	5	2	11	2	2 and 3
	$n_j = yz + \lvert x - z \rvert$; $s_j = y$;							
$x = y > z$	$w_j = y - z$; $u_j = x$		2	2	1	3	2	1 and 2
			3	3	2	7	4	2 and 3
$y < z < x$			3	1	2	3	1	0 and 3
			4	2	3	7	2	3 and 4
$z < y < x$			3	2	1	4	2	1 and 3
			5	3	2	9	3	2 and 5
$y = z < x$			3	1	1	3	1	0 and 3
			4	2	2	6	2	2 and 4

Battery configurations that do not meet the mass, m_{sys}, volume, v_{sys}, or areal footprint, a_{sys} targets are eliminated, by our algorithm, from the list of potential cell configurations. If no batteries remain after this elimination step, battery configurations having the least mass, volume, or areal (depending on user specification) values are selected.

3.7. Selection based on specific energy or energy density

If volume prioritization is selected by the user, energy density is computed using the expression:

$$\hat{E}_j = \frac{E_j}{\hat{V}_j} \tag{33}$$

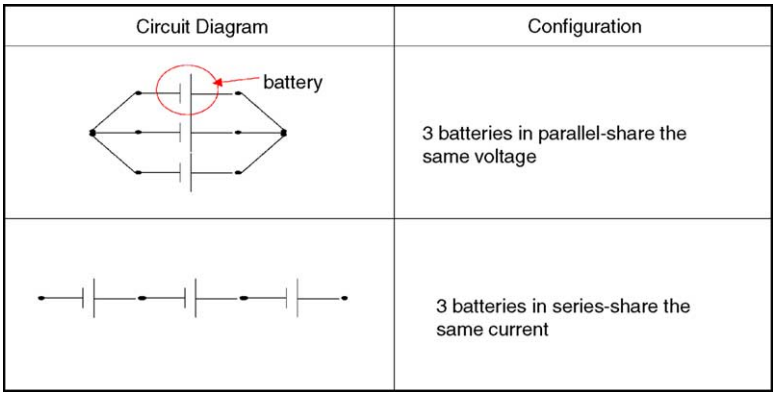

Fig. 2. Circuit diagrams illustrating batteries in both parallel and series.

for the remaining batteries. Cell configurations providing the maximum energy density are selected next. If mass prioritization is selected, battery selection is based on specific energy as:

$$\check{E}_j = \frac{E_j}{M_j} \tag{34}$$

where the maximum specific energy generated from this expression corresponded to battery(s) selected.

3.8. Selection based on battery lifetime

If more than one battery remains after application of all previous constraints, then they were subjected to evaluation of lifetime. Configurations providing the longest battery lifetime for a particular approach are used. This lifetime is:

$$L_j = t_{\text{final}}(\rho)(\bar{N}_j) \tag{35}$$

where ρ equal to 1 for primary cells or equal to the number of cycles a secondary battery can provide. The final results for each approach are compared and an optimal solution is selected.

3.9. WIMS/ERC testbed

Power and voltage requirements for components of the WIMS–EMT are listed in Table 2. User input parameters are listed in Table 6. Since no environmental constraints were provided for the WIMS–EMT for discharge and charge temperature, charge rate, method of charge, storage time, etc., all battery electrochemistries were considered potential candidates, and the algorithm analysis began with calculation of device parameters.

4. Results

4.1. Approach 1

4.1.1. Calculated device parameters

Energy and power data for each device was summed per time segment to produce aggregate system parameters for Approach 1. These values for energy (0.39 Wh), weighted power (1.42 W), specific energy (91.06 Wh kg^{-1}), energy density (270.04 Wh L^{-1}), specific power (330.49 W kg^{-1}), and power density (980.0 W L^{-1}) system are listed in Table 7.

Table 6
EMT input constants and power supply design targets

Number of device in the systems, N	10
Ambient temperature [°C]	20
[p]rimary or [s]econdary battery system	S
[v]olume or [m]ass optimization	M
Desired mass [kg]	0.0043
Desired volume [cm^3]	1.45
Number of cycles	1
Number of power bundles, n_{loc}	4
Mass [kg] μW range, m_1	0.000086
Mass [kg] mW range, m_2	0.00077
Mass W range, m_3	0.00344
Volume [cm^3] μW range, v_1	0.029
Volume [cm^3] mW range, v_2	0.261
Volume [cm^3] W range, v_3	0.00344
Volume [cm^3]–bundle 1	3.68
Area [cm^2]—bundle 2	61.0

4.1.2. Calculation of energy, voltage, and current factors—application of conditionality statements

For each of the 25 batteries in the database, energy (x_j), voltage (y_j), and current (z_j) factors were computed; along with the total number of batteries required, n_j, number in series, s_j, number in parallel, w_j, configuration mass, M_j, volume, $\hat{V}_j$, number of cycles, $\bar{N}_j$, and lifetime, L_j. The results from these calculations are listed in Table 8.

4.1.3. Selection based on mass requirements

The WIMS–EMT requires mass prioritization, where the target mass of the power system is 0.0043 kg. Clearly, from the results listed in Table 8, no battery system in the database met this target value, so the systems producing the minimum mass values of 0.068 and 0.069 kg (Ultralife UBC641730/PCM and UBP383450/PCM) were selected. For the Ultralife UBC641730/PCM, 15 batteries were required ($n = 15$), with 5 in series ($s = 5$), in 3 parallel rows ($w = 3$). Selection of the Ultralife UBP383450/PCM configuration required $n = 5$; all were placed in series ($s = 5$). A basic circuit diagram of the power system design based on Approach 1 is detailed in Fig. 3.

Table 7
Approach 1: power and energy values as a function of time

Time	Power (Watts)	Calculated voltage (V)	Current (A)	Energy (Wh)	Specific energy (Wh kg^{-1})	Energy density (Wh L^{-1})	Weighted power (W)	Specific power (W kg^{-1})	Power density (W L^{-1})	Maximum voltage (V)
5	1.125	3.438	0.327	0.002	0.363	1.077	0.006	1.319	3.911	6
555	1.115	3.527	0.316	0.172	39.959	118.499	0.624	145.073	430.218	6
3	4.735	9.252	0.512	0.004	0.918	2.722	0.014	3.330	9.876	17
9	1.91	5.56	0.344	0.005	1.112	3.298	0.017	4.030	11.951	15
420	1.795	3.869	0.464	0.209	48.707	144.443	0.760	176.739	524.124	15
992	10.68		Total	0.392	91.060	270.039	1.421	330.492	980.079	

Mass (kg) = 0.0043; volume (L) = 0.00145.

Table 8
Results generated from application of Approach 1

Approach 1 - grouping aggregate power supply curve																
Electrochemistry	Part Number	Discharge Current (A)	Energy [Wh]	Nominal Voltage (V)	x (energy ratio)	y (voltage ratio)	z (current ratio)	n (number of batteries)	s (series)	w (parallel)	M (kg)	$\hat{V}_j(L)$	Number of Cycles (not including recharge cycles)	Lifetime [h]	Specific Energy [Wh/kg]	Energy Density [Wh/L]
Manganese Lithium	ML414S	5.00E-06	0.004	3.0	108.78	5.67	102400.00	614400.00	6.00	102400.00	49.152	15.565	5648	1.62E+06	45.00	142.10
	ML421S	3.00E-06	0.007	3.0	56.75	5.67	170666.67	1024002.00	6.00	170667.00	112.640	38.913	18043	5.17E+06	62.73	181.58
Nickel Metal Hydride	HHR60AAAH	0.10	0.600	1.2	0.65	14.17	5.12	90.00	15.00	6.00	1.080	0.347	138	1.98E+04	50.00	155.71
	HHR70AAAJ	0.14	0.864	1.2	0.45	14.17	3.56	60.00	15.00	4.00	0.780	0.231	132	1.90E+04	66.46	224.23
	NH50-D	0.50	3.000	1.2	0.13	14.17	1.02	30.00	15.00	2.00	2.190	1.695	230	3.29E+04	41.10	53.10
	NH35-C	0.50	3.000	1.2	0.13	14.17	1.02	30.00	15.00	2.00	1.800	0.809	230	3.29E+04	50.00	111.29
	NH12-AAA	0.17	1.020	1.2	0.38	14.17	3.01	60.00	15.00	4.00	0.720	0.231	156	2.24E+04	85.00	264.71
	NH15-AA	0.46	2.760	1.2	0.14	14.17	1.11	30.00	15.00	2.00	0.810	0.250	211	3.03E+04	102.22	330.97
	NH22-9V	0.03	0.180	1.2	2.18	14.17	17.07	270.00	15.00	18.00	11.070	5.865	124	1.78E+04	4.39	8.29
	SP75AAAMH	0.15	0.900	1.2	0.44	14.17	3.41	60.00	15.00	4.00	0.780	0.200	138	1.98E+04	69.23	269.63
	SP180AAKH	0.36	2.160	1.2	0.18	14.17	1.42	30.00	15.00	2.00	0.840	0.238	165	2.37E+04	77.14	272.78
	SP230AAKH	0.46	2.760	1.2	0.14	14.17	1.11	30.00	15.00	2.00	0.900	0.231	211	6.06E+04	92.00	358.59
Lithium Ion	CGR17500	0.16	2.988	3.6	0.13	4.72	3.28	20.00	5.00	4.00	0.500	0.223	153	2.19E+04	119.52	268.56
	CGR18650HG	0.34	6.480	3.6	0.06	4.72	1.51	10.00	5.00	2.00	0.420	0.175	165	2.37E+04	154.29	370.88
	UBC641730/PCM	**0.19**	**0.74**	**3.7**	**0.53**	**4.59**	**2.69**	**15**	**5**	**3**	**0.068**	**0.058**	**28**	**2437.72**	**164.44**	**192.20**
	UBP383450/PCM	**0.59**	**2.220**	**3.7**	**0.18**	**4.59**	**0.87**	**5.00**	**5.00**	**1.00**	**0.069**	**0.043**	**28**	**4.06E+03**	**160.87**	**259.54**
	UBC422030/PCM	0.14	0.555	3.7	0.71	4.59	3.66	20.00	5.00	4.00	0.080	0.061	28	2.44E+03	138.75	181.39
	ICP383450G	0.14	2.590	3.7	0.15	4.59	3.66	20.00	5.00	4.00	0.290	0.132	132	1.90E+04	178.62	393.01
	ICP043048G	0.14	2.664	3.7	0.15	4.59	3.56	20.00	5.00	4.00	0.290	0.130	136	1.95E+04	183.72	410.70
	CGA523450A	0.90	3.276	3.6	0.12	4.72	0.57	5	5	1	0.098	0.045	42	5995.47	168.00	367.06
	CGA523436	0.68	2.520	3.6	0.16	4.72	0.75	5.00	5.00	1.00	0.073	0.032	32	4.61E+03	173.79	395.93
Nickel Cadmium	P-11AAH	0.02	0.144	1.2	2.72	14.17	21.33	330.00	15.00	22.00	2.145	0.954	121	1.74E+04	22.15	49.83
	P-18N	0.04	0.228	1.2	1.72	14.17	13.47	210.00	15.00	14.00	1.680	0.713	122	1.75E+04	28.50	67.20
	SP30AA2/3MC	1.50	0.360	1.2	1.09	14.17	0.34	15.00	15.00	1.00	0.165	0.068	14	1.98E+03	32.73	79.76
	SP28AAAMC	1.40	0.336	1.2	1.17	14.17	0.37	15.00	15.00	1.00	0.135	0.052	13	1.84E+03	37.33	96.98

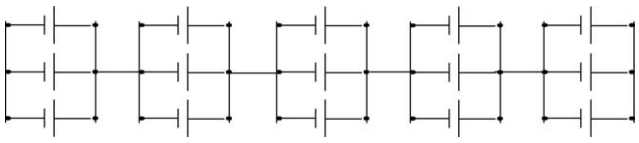

Fig. 3. Circuit diagram for solution proposed from Approach 1.

4.1.4. Selection based on specific energy

Of the two battery systems examined, the Ultralife UBC641730/PCM had the highest specific energy, 164.44 Wh kg^{-1}, although its predicted lifetime (2.4E03 h) was much less than a system designed using the UBP383450/PCM cell (4.1E03 h).

4.1.5. Selection based on battery lifetime

Ultralife UBP383450/PCM battery provided a longer life (4.1E03 h) in comparison to UBC641730/PCM (2.4E03 h). The resulting total number of batteries needed is 15, and the total mass and volume of the power system is 0.068 kg and 0.058 L, respectively.

4.2. Approach 2

4.2.1. Calculated system parameters

The WIMS–EMT device power and energy values are summarized in Table 9. Arrangement #2 was chosen so that the power range for the mW section was less than 1 W; subdevices with the largest power values in the milliwatt range were moved from the milliwatt power range to the watt power range. Energy, power, specific energy, and energy density values for each power range are shown in Table 10. Energy, power, specific energy, and energy density values for each power range are shown in Table 10. Resulting energy and power values for the μW range were 0.023 μWh and 0.085 mW, respectively, and the specific energy and energy density values were 0.271 Wh kg^{-1} and 0.803 Wh L^{-1}, respectively. The energy and power values for the mW range were 0.13 Wh and 0.47 W, respectively, and the specific energy and energy density values 168.048 Wh kg^{-1} and 498.350 Wh L^{-1}. Lastly, energy and weighted power values for the watt power range were 0.27 Wh and 0.99 W, respectively, and the specific energy and energy density values were 79.275 Wh kg^{-1} and 287.690 Wh L^{-1}.

4.2.2. Calculation of energy, voltage, and current factors—application of conditionality statements

Research on development of high-power and capacity thin film and microbattery technologies has intensified in recent years (e.g. [9,10,27,18]). We studied implementation of lithium-free thin film batteries proposed by Neudecker et al. [27], for the power source for the micro-watt power range. According to Neudecker et al. [27], these batteries have the capability of cycling between 4.2 and 3.0 V, and have demonstrated 1000 cycles at 1 mA/cm^2, or over 500 cycles at 5 mA/cm^2. Also when operated below 0.1 mA/cm^2, they provided a capacity of about 200 mAh/cm^2 from a Li-free battery with 3.2 mm thick $LiCoO_2$ cathode. Hence, this battery technology was added to the 25 commercial batteries in the database for the power selection for the μW power range. The energy (x_j), voltage (y_j), and current (z_j) factors were computed; along with the total number of batteries required, n_j number in series, s_j, number in parallel, w_j, configuration mass, M_j, volume, $\hat{V}_j$, number of cycles, $\bar{N}_j$, and lifetime, L_j for the all power ranges. The results for the μW, mW, and W ranges are detailed in Table 11(a–c), respectively.

4.2.3. Selection based on mass requirements

The thin-film technology is the obvious choice for the μW power range, as its mass and volume are very small, and its surface area is 1 cm^2. A lithium polymer cells, UBC422030/PCM and UBC641730/PCM provided the smallest power system mass values: 0.008 and 0.009 kg for the mW power range. Also two lithium polymer batteries, UBC641730/PCM and UBC422030/PCM provided the lowest mass results for the W power range as well, 0.023 and 0.040 kg, respectively.

4.2.4. Selection based on specific energy requirements

Of the two batteries proposed for the mW power range, the UBC641730/PCM battery is selected because its specific energy, 164.44 Wh kg^{-1} is greater than the specific energy of

Table 9
Arrangements #1 and #2 for Approach 2

Arrangement #1				Arrangement #2			
Power range	Device list	Power (mW)	Total energy (mWh)	Power range	Device list	Power (mW)	Total energy (mWh)
μW	GC sensor array	0.085	0.023	μW	GC sensor array	0.085	0.023
mW	TE cooler, microvalves, MCU, vacuum pump, RF board, column #1, column #2, preconcentrator	1294	357	mW	TE cooler, microvalves MCU, RF board	472	130
W	Preconcentrator	11	3	W	Column #1, column #2, preconcentrator, vacuum pump	990	273

Table 10
Approach 2: micro, milli, and Watt range power and energy values as a function of time

Time	Microwatt range current (A)	Microwatt range (W)	Calculated voltage (V)	Energy (Wh)	Weighted power (W)	Specific energy (Wh kg^{-1})	Energy density (Wh L^{-1})	Specific power (W kg^{-1})	Energy density (Wh L^{-1})
Microwatt range									
613	0	0	0.00	0.00	0.00	0.00	0.00	0.00	0.00
419	6.67E−05	2.00E−04	3.0	2.33E−05	0.0001	0.27	0.80	0.98	2.91
Time	Discharge current (A)	Milliwatt power (W)	Energy (Wh)	Weighted power (W)	Specific energy (Wh kg^{-1})	Energy density (Wh L^{-1})	Specific power (W kg^{-1})	Power density (W L^{-1})	
Milliwatt range[a]									
5	0.0022	0.3470	0.0005	0.0017	168.05	498.35	609.85	1808.53	
555	0.12795	0.34500	0.0532	0.1930					
3	0.12795	0.34500	0.0003	0.0010					
9	0.12795	0.34500	0.0009	0.0031					
420	0.23469	0.64500	0.0753	0.2731					
		Total	0.13	0.47					
Time	Discharge current (A)	Milliwatt power (W)	Energy (Wh)	Weighted power (W)	Specific energy (Wh kg^{-1})	Energy density (Wh L^{-1})	Specific power (W kg^{-1})	Power density (W L^{-1})	
Watt range[b]									
5	0.12987	0.78000	0.0011	0.0039	79.27	235.09	287.69	853.15	
555	0.12987	0.78000	0.1203	0.4364					
3	0.13051	4.48000	0.0037	0.0135					
9	0.13652	1.65500	0.0041	0.0150					
420	0.14216	1.23000	0.1435	0.5208					
		Total	0.27	0.99					

[a] m_2 (kg) = 0.000774, v_2 (L) = 0.0003, V_2 (V) = 3.0.
[b] m_1 (kg) = 0.00344, v_1 (L) = 0.0012, V_1 (V) = 17.0.

UBC422030/PCM, 138.75. Also, battery UBC641730/PCM provided sufficiently greater lifetime (979 h) compared to UBC422030/PCM (734 h). For mW power range, where UBC641730/PCM is used, $n_2 = 2$, $s_2 = 1$, and $w_2 = 2$, indicating that a total of two batteries are required to be placed in parallel for the mW power range. Of the two batteries proposed for the W power range, UBC422030/PCM and UBC641730/PCM, the latter provides the largest specific energy, 164 Wh kg^{-1} compared to 139 Wh kg^{-1} provided by UBC422030/PCM. The UBC422030/PCM, however, does provide a longer battery life (1.75E03 h) in comparison to UBC641730/PCM (1.17E03 h). For this power range, $n_3 = 5$, $s_3 = 5$, and $w_3 = 1$, wherein a total of five batteries are required to be placed in series.

4.2.5. Selection based on battery lifetime

All battery electrochemistry and type selection were determined in Section 4.2.4, however, since this is a hybrid system, battery lifetimes vary depending on the power range. The battery lifetime predicted for the μW, mW, and W power ranges are 8.89E03, 979, and 164 h. The total number of batteries required is eight, wherein the total mass and volume of the power system based on Approach 2 is 0.032 kg and 0.028 L, respectively.

4.3. Approach 3

4.3.1. Calculated parameters

The largest surface area available for application of batteries on the WIMS–EMT is 60.1 cm^2, along the bottom of the PC Board. Since packaging is still under development, we use this area to define one power bundle, and designate one other location for a high-energy density battery that can potentially be stacked on top of the device or along side of the device, where the volume will be limited to 1/4 (3.7 cm^3) the size of the fluidic substrate which spans the entire length of the device. The strategy is to use a thin-film battery to assist in providing current for the high-power pulses of the power versus time curve and to use a high-energy density cell to provide the moderate current loads. A schematic demonstrating the concept of grouping power supplies by location is depicted in Fig. 4. The amount of energy required to supply bundle 1 is 0.38 Wh and the weighted power is 1.38 W (Table 12). Hence, estimates for the energy and power densities are 103.6 and 376.6 W L^{-1} for bundle 1, respectively. The energy and weighted power for bundle 1 are 0.08 and 0.17 W, respectively. The energy per unit area and power per unit area required for bundle 2 are 8E–04 and 2.8E–03 W cm^{-2}.

Table 11
Results from application of Approach 2 (a) microwatt (b) milliwatt (c) watt power ranges

Microwatt Power Range

Electrochemistry	Part Number	Discharge Current (A)	Energy [Wh]	Nominal Voltage (V)	x	y	z	n	s	w	M (kg)	V (L)	area(cm^2)	Number of Cycles (not including recharge cycles)	Lifetime	Energy Density [Wh/cm^2]
Lithium Fee Thin-Film Battery	-	1.00E-04	7.2E-01	3.60	0.00	0.83	0.67	1	1	1	-	-	1	30930.79	8.87E+06	0.720
Electrochemistry	Part Number	Discharge Current (A)	Energy [Wh]	Nominal Voltage (V)	x (energy ratio)	y (voltage ratio)	z (current ratio)	n (number of batteries)	s (series)	w (parallel)	M (kg)		Number of Cycles (not including recharge cycles)	Lifetime [h]	Specific Energy [Wh/kg]	Energy Density [Wh/L]
Manganese Lithium	ML414S	5.00E-06	0.004	3.0	6.47E-03	1.0	13.3	14	1.0	14.0	0.001	3.55E-04	2165.2	6.21E+05	45.00	142.10
	ML421S	3.00E-06	0.007	3.0	3.37E-03	1.0	22.2	23	1.0	23.0	0.003	8.74E-04	6817.7	1.95E+06	62.73	181.58
Nickel Metal Hydride	HHR60AAAH	1.00E-01	0.600	1.2	3.88E-05	2.5	6.67E-04	3	3.0	1.0	0.036	1.16E-02	77327.0	1.11E+07	50.00	155.71
	HHR70AAAJ	1.44E-01	0.864	1.2	2.69E-05	2.5	4.63E-04	3	3.0	1.0	0.039	1.16E-02	111350.8	1.60E+07	66.46	224.23
	NH50-D	5.00E-01	3.000	1.2	7.76E-06	2.5	1.33E-04	3	3.0	1.0	0.219	1.69E-01	386634.8	5.54E+07	41.10	53.10
	NH35-C	5.00E-01	3.000	1.2	7.76E-06	2.5	1.33E-04	3	3.0	1.0	0.180	8.09E-02	386634.8	5.54E+07	50.00	111.29
	NH12-AAA	1.70E-01	1.020	1.2	2.28E-05	2.5	3.92E-04	3	3.0	1.0	0.036	1.16E-02	131455.8	1.88E+07	85.00	264.71
	NH15-AA	4.60E-01	2.760	1.2	8.43E-06	2.5	1.45E-04	3	3.0	1.0	0.081	2.50E-02	355704.1	5.10E+07	102.22	330.97
	NH22-9V	3.00E-02	0.180	1.2	1.29E-04	2.5	2.22E-03	3	3.0	1.0	0.123	6.52E-02	23198.1	3.33E+06	4.39	8.29
	SP75AAAMH	1.50E-01	0.900	1.2	2.59E-05	2.5	4.44E-04	3	3.0	1.0	0.039	1.00E-02	115990.5	1.66E+07	69.23	269.63
	SP180AAKH	3.60E-01	2.160	1.2	1.08E-05	2.5	1.85E-04	3	3.0	1.0	0.084	2.38E-02	278377.1	3.99E+07	77.14	272.78
	SP230AAKH	4.60E-01	2.760	1.2	8.43E-06	2.5	1.45E-04	3	3.0	1.0	0.090	2.31E-02	355704.1	1.02E+08	92.00	358.59
Lithium Ion	CGR17500	1.56E-01	2.988	3.6	7.79E-06	0.8	4.27E-04	1	1.0	1.0	0.025	1.11E-02	128362.8	1.84E+07	119.52	268.56
	CGR18650HG	3.40E-01	6.480	3.6	3.59E-06	0.8	1.96E-04	1	1.0	1.0	0.042	1.75E-02	278377.1	3.99E+07	154.29	370.88
	UBC641730/PCM	1.50E-01	0.740	3.7	3.15E-05	0.8	4.44E-04	1	1.0	1.0	0.005	3.85E-03	31790.0	2.73E+06	164.44	192.20
	UBP383450/PCM	3.00E-01	2.220	3.7	1.05E-05	0.8	2.22E-04	1	1.0	1.0	0.014	8.55E-03	95369.9	1.37E+07	160.87	259.54
	UBC422030/PCM	7.50E-02	0.555	3.7	4.19E-05	0.8	8.89E-04	1	1.0	1.0	0.004	3.06E-03	23842.5	2.05E+06	138.75	181.39
	ICP383450G	1.40E-01	2.590	3.7	8.99E-06	0.8	4.76E-04	1	1.0	1.0	0.015	6.59E-03	111264.9	1.59E+07	178.62	393.01
	ICP043048G	1.44E-01	2.664	3.7	8.74E-06	0.8	4.63E-04	1	1.0	1.0	0.015	6.49E-03	114443.9	1.64E+07	183.72	410.70
	CGA523450A	0.9	3.3	3.6	7.11E-06	0.8	7.41E-05	1	1.0	1.0	0.020	8.93E-03	140735.1	2.02E+07	168.00	367.06
	CGA523436	0.7	2.5	3.6	9.24E-06	0.8	9.80E-05	1	1.0	1.0	0.015	6.36E-03	108257.8	1.55E+07	173.79	395.93
Nickel Cadmium	P-11AAH	2.40E-02	0.144	1.2	1.62E-04	2.5	2.78E-03	3	3.0	1.0	0.020	8.67E-03	18558.5	2.66E+06	22.15	49.83
	P-18N	3.80E-02	0.228	1.2	1.02E-04	2.5	1.75E-03	3	3.0	1.0	0.024	1.02E-02	29384.2	4.21E+06	28.50	67.20
	SP30AA2/3MC	1.50E+00	0.360	1.2	6.47E-05	2.5	4.44E-05	3	3.0	1.0	0.033	1.35E-02	46396.2	6.65E+06	32.73	79.76
	SP28AAAMC	1.40E+00	0.336	1.2	6.93E-05	2.5	4.76E-05	3	3.0	1.0	0.027	1.04E-02	43303.1	6.21E+06	37.33	96.98

Table 11 (*Continued*)

Milliwatt Power Range

Electrochemistry	Part Number	Discharge Current (A)	Energy [Wh]	Nominal Voltage (V)	x (energy ratio)	y (voltage ratio)	z (current ratio)	n (number of batteries)	s (series)	w (parallel)	M (kg)	$\hat{V}_j(L)$	Number of Cycles (not including recharge cycles)	Lifetime [h]	Specific Energy [Wh/kg]	Energy Density [Wh/L]
Manganese Lithium	ML414S	5.00E-06	0.004	3.0	36.13	1.0	46938.6	46939	1.0	46939.0	3.755	1.189	1299.2	3.72E+05	45.00	142.10
	ML421S	3.00E-06	0.007	3.0	18.85	1.0	78231.0	78232	1.0	78232.0	8.606	2.973	4150.1	1.19E+06	62.73	181.58
Nickel Metal Hydride	HHR60AAAH	1.00E-01	0.600	1.2	0.22	2.5	2.3	9	3.0	3.0	0.108	0.035	41.5	5.95E+03	50.00	155.71
	HHR70AAAJ	1.44E-01	0.864	1.2	0.15	2.5	1.6	6	3.0	2.0	0.078	0.023	39.9	5.71E+03	66.46	224.23
	NH50-D	5.00E-01	3.000	1.2	0.04	2.5	0.5	3	3.0	1.0	0.219	0.169	69.2	9.92E+03	41.10	53.10
	NH35-C	5.00E-01	3.000	1.2	0.04	2.5	0.5	3	3.0	1.0	0.180	0.081	69.2	9.92E+03	50.00	111.29
	NH12-AAA	1.70E-01	1.020	1.2	0.13	2.5	1.4	6	3.0	2.0	0.072	0.023	47.1	6.74E+03	85.00	264.71
	NH15-AA	4.60E-01	2.760	1.2	0.05	2.5	0.5	3	3.0	1.0	0.081	0.025	63.7	9.12E+03	102.22	330.97
	NH22-9V	3.00E-02	0.180	1.2	0.72	2.5	7.8	24	3.0	8.0	0.984	0.521	33.2	4.76E+03	4.39	8.29
	SP75AAAMH	1.50E-01	0.900	1.2	0.14	2.5	1.6	6	3.0	2.0	0.078	0.020	41.5	5.95E+03	69.23	269.63
	SP180AAKH	3.60E-01	2.160	1.2	0.06	2.5	0.7	3	3.0	1.0	0.084	0.024	49.8	7.14E+03	77.14	272.78
	SP230AAKH	4.60E-01	2.760	1.2	0.05	2.5	0.5	3	3.0	1.0	0.090	0.023	63.7	1.82E+04	92.00	358.59
Lithium Ion	CGR17500	1.56E-01	2.988	3.6	0.04	0.8	1.5	2	1.0	2.0	0.050	0.022	45.9	6.59E+03	119.52	268.56
	CGR18650HG	3.40E-01	6.480	3.6	0.02	0.8	0.7	1	1.0	1.0	0.042	0.017	49.8	7.14E+03	154.29	370.88
	UBC641730/PCM	**1.90E-01**	**0.740**	**3.7**	**0.18**	**0.8**	**1.2**	**2**	**1.0**	**2.0**	**0.009**	**0.008**	**11.4**	**9.79E+02**	**164.44**	**192.20**
	UBP383450/PCM	**5.90E-01**	**2.220**	**3.7**	**0.06**	**0.8**	**0.4**	**1**	**1.0**	**1.0**	**0.014**	**0.009**	**17.1**	**2.45E+03**	**160.87**	**259.54**
	UBC422030/PCM	**1.40E-01**	**0.555**	**3.7**	**0.23**	**0.8**	**1.7**	**2**	**1.0**	**2.0**	**0.008**	**0.006**	**8.5**	**7.34E+02**	**138.75**	**181.39**
	ICP383450G	1.40E-01	2.590	3.7	0.05	0.8	1.7	2	1.0	2.0	0.029	0.013	39.8	5.71E+03	178.62	393.01
	ICP043048G	1.44E-01	2.664	3.7	0.05	0.8	1.6	2	1.0	2.0	0.029	0.013	41.0	5.87E+03	183.72	410.70
	CGA523450A	0.9	3.3	3.6	0.04	0.8	0.3	1	1.0	1.0	0.020	0.009	25.2	3.61E+03	168.00	367.06
	CGA523436	0.7	2.5	3.6	0.05	0.8	0.3	1	1.0	1.0	0.015	0.006	19.4	2.78E+03	173.79	395.93
Nickel Cadmium	P-11AAH	2.40E-02	0.144	1.2	0.90	2.5	9.8	30	3.0	10.0	0.195	0.087	33.2	4.76E+03	22.15	49.83
	P-18N	3.80E-02	0.228	1.2	0.57	2.5	6.2	21	3.0	7.0	0.168	0.071	36.8	5.28E+03	28.50	67.20
	SP30AA2/3MC	1.50E+00	0.360	1.2	0.36	2.5	0.2	3	3.0	1.0	0.033	0.014	8.3	1.19E+03	32.73	79.76
	SP28AAAMC	1.40E+00	0.336	1.2	0.39	2.5	0.2	3	3.0	1.0	0.027	0.010	7.7	1.11E+03	37.33	96.98

Table 11 (*Continued*)

Watt Power Range

Electrochemistry	Part Number	Discharge Current (A)	Energy [Wh]	Nominal Voltage (V)	x (energy ratio)	y (voltage ratio)	z (current ratio)	n (number of batteries)	s (series)	w (parallel)	M (kg)	$\hat{V}_j(L)$	Number of Cycles (not including recharge cycles)	Lifetime [h]	Specific Energy [Wh/kg]	Energy Density [Wh/L]
Manganese Lithium	ML414S	5.00E-06	0.004	3.0	75.75	5.7	2.84E+04	1.71E+05	6.0	28432.0	13.647	4.32	2.25E+03	6.46E+05	4.50E+01	1.42E+02
	ML421S	3.00E-06	0.007	3.0	39.52	5.7	4.74E+04	2.84E+05	6.0	47387.0	31.275	10.80	7.19E+03	2.06E+06	6.27E+01	1.82E+02
Nickel Metal Hydride	HHR60AAAH	1.00E-01	0.600	1.2	0.45	14.2	1.42E+00	3.00E+01	15.0	2.0	0.360	0.12	6.60E+01	9.46E+03	5.00E+01	1.56E+02
	HHR70AAAJ	1.44E-01	0.864	1.2	0.32	14.2	9.87E-01	1.50E+01	15.0	1.0	0.195	0.06	4.75E+01	6.81E+03	6.65E+01	2.24E+02
	NH50-D	5.00E-01	3.000	1.2	0.09	14.2	2.84E-01	15.0	15.0	1.0	1.095	0.85	1.65E+02	2.37E+04	4.11E+01	5.31E+01
	NH35-C	5.00E-01	3.000	1.2	0.09	14.2	2.84E-01	15.0	15.0	1.0	0.900	0.40	1.65E+02	2.37E+04	5.00E+01	1.11E+02
	NH12-AAA	1.70E-01	1.020	1.2	0.27	14.2	8.36E-01	15.0	15.0	1.0	0.180	0.06	5.61E+01	8.04E+03	8.50E+01	2.65E+02
	NH15-AA	4.60E-01	2.760	1.2	0.10	14.2	3.09E-01	15.0	15.0	1.0	0.405	0.13	1.52E+02	2.18E+04	1.02E+02	3.31E+02
	NH22-9V	3.00E-02	0.180	1.2	1.52	14.2	4.74E+00	75.0	15.0	5.0	3.075	1.63	4.95E+01	7.10E+03	4.39E+00	8.29E+00
	SP75AAAMH	1.50E-01	0.900	1.2	0.30	14.2	9.48E-01	15.0	15.0	1.0	0.195	0.05	4.95E+01	7.10E+03	6.92E+01	2.70E+02
	SP180AAKH	3.60E-01	2.160	1.2	0.13	14.2	3.95E-01	15.0	15.0	1.0	0.420	0.12	1.19E+02	1.70E+04	7.71E+01	2.73E+02
	SP230AAKH	4.60E-01	2.760	1.2	0.10	14.2	3.09E-01	15.0	15.0	1.0	0.450	0.12	1.52E+02	4.35E+04	9.20E+01	3.59E+02
Lithium Ion	CGR17500	0.16	2.988	3.6	0.09	4.7	9.11E-01	5.0	5.0	1.0	0.125	0.06	5.48E+01	7.85E+03	1.20E+02	2.69E+02
	CGR18650HG	0.34	6.480	3.6	0.04	4.7	4.18E-01	5.0	5.0	1.0	0.210	0.09	1.19E+02	1.70E+04	1.54E+02	3.71E+02
	UBC641730/PCM	**0.19**	**0.740**	**3.7**	**0.37**	**4.6**	**7.48E-01**	**5.0**	**5.0**	**1.0**	**0.023**	0.02	**1.36E+01**	**1.17E+03**	**1.64E+02**	**1.92E+02**
	UBP383450/PCM	0.59	2.220	3.7	0.12	4.6	2.41E-01	5.0	5.0	1.0	0.069	0.04	4.07E+01	5.83E+03	1.61E+02	2.60E+02
	UBC422030/PCM	**0.14**	**0.555**	**3.7**	**0.49**	**4.6**	**1.02E+00**	**10.0**	**5.0**	**2.0**	**0.040**	0.03	**2.04E+01**	**1.75E+03**	**1.39E+02**	**1.81E+02**
	ICP383450G	0.14	2.590	3.7	0.11	4.6	1.02E+00	10.0	5.0	2.0	0.145	0.07	9.50E+01	1.36E+04	1.79E+02	3.93E+02
	ICP043048G	0.14	2.664	3.7	0.10	4.6	9.87E-01	5.0	5.0	1.0	0.073	0.03	4.88E+01	7.00E+03	1.84E+02	4.11E+02
	CGA523450A	0.90	3.3	3.6	0.08	4.7	1.58E-01	5.0	5.0	1.0	0.098	0.04	6.01E+01	8.61E+03	1.68E+02	3.67E+02
	CGA523436	0.68	**2.5**	**3.6**	**0.11**	**4.7**	**2.09E-01**	**5.0**	**5.0**	**1.0**	**0.073**	0.03	**4.62E+01**	**6.62E+03**	**1.74E+02**	**3.96E+02**
Nickel Cadmium	P-11AAH	2.40E-02	0.144	1.2	1.89	14.2	5.92E+00	90.0	15.0	6.0	0.585	0.26	4.75E+01	6.81E+03	2.22E+01	4.98E+01
	P-18N	3.80E-02	0.228	1.2	1.20	14.2	3.74E+00	60.0	15.0	4.0	0.195	0.20	5.02E+01	7.19E+03	7.02E+01	6.72E+01
	SP30AA2/3MC	1.50E+00	0.360	1.2	0.76	14.2	9.48E-02	15.0	15.0	1.0	0.165	0.07	1.98E+01	2.84E+03	3.27E+01	7.98E+01
	SP28AAAMC	1.40E+00	0.336	1.2	0.81	14.2	1.02E-01	15.0	15.0	1.0	0.195	0.05	1.85E+01	2.65E+03	2.58E+01	9.70E+01

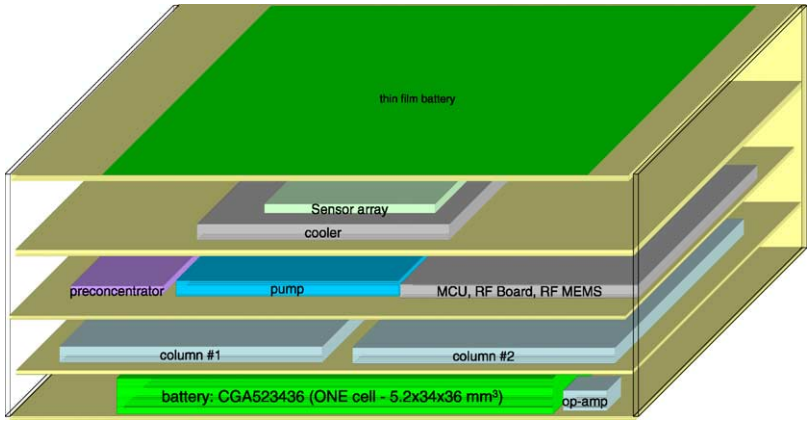

Fig. 4. Schematic illustrating implementation of Approach 3, grouping by power site location.

Table 12
Approach 3: power and energy data for power bundle sites

Time	Power (Watts)	Calculated voltage (V)	Current (A)	Energy (Wh)	Weighted power (W)	Maximum voltage (V)	Power density ($W L^{-1}$)	Energy density ($Wh L^{-1}$)
Power bundle #1[a]								
5	1.089846	3.438	0.317	0.002	0.005	6	376.571	103.766
555	1.079262	3.527	0.306	0.166	0.604	6		
3	4.644504	9.252	0.502	0.004	0.014	17		
9	1.85704	5.56	0.334	0.005	0.017	15		
420	1.756526	3.869	0.454	0.205	0.744	15		
992			Total	0.381	1.384			
Bundle 2 current (A)	Bundle 2 power (W)	Energy (Wh)	Weighted power (W)	Energy density ($Wh cm^{-2}$)	Power density ($W cm^{-2}$)			
Power bundle #2[b]								
0.06	1.02	2.92E − 01	1.02	4.79E − 03	1.67E − 2			

[a] v_1 (L) = 3.68E − 03, V_1 (V) = 17.
[b] a_2 (cm^2) = 6.10E + 01, V_2 (V) = 17.0.

4.3.2. Calculation of energy, voltage, and current factors–application of conditionality statements

The maximum number of thin films available for use is 60 wherein each film is approximately 1 cm^2 and is capable of providing 5 mA/cm^2. The energy (x_j), voltage (y_j), and current (z_j) factors were computed; along with the total number of batteries required, n_j, number in series, s_j, number in parallel, w_j, configuration mass, M_j, volume, $\hat{V}_j$, number of cycles, $\bar{N}_j$, and lifetime, L_j for all the power bundle locations and the results are in Table 13(a and b) for bundle 1 and 2, respectively.

4.3.3. Selection based on mass requirements

Results for Approach 3 are listed in Table 13(a) bundle 1 and (b) bundle 2. The minimum masses for bundle 1 are obtained from UBC641730/PCM (0.068 kg), UBP383450/PCM (0.069 kg), and CGA523436 (0.073 kg). Thin-film lithium-free batteries are used for bundle 2.

4.3.4. Selection based on specific energy requirements

The Panasonic battery, CGA523436 (0.073 kg), was selected for two reasons. First, it had the highest specific energy (173.70 Wh kg^{-1}) of the all three batteries, and the smallest volume.

4.3.5. Selection based on battery lifetime

All battery electrochemistry and type selection are completed in Section 4.3.3, however, since this is a hybrid system, battery lifetimes vary depending on the power bundle. The battery lifetime predicted for bundles 1 and 2 are 2.1E04 and 4.74E03 h, respectively. The resulting total number of batteries required is 65, and the total mass and volume of the power system is 0.073 kg and 0.032 L.

5. Implementation of operational amplifier (op-amp) and voltage generator technology

The methodology detailed here assumes no implementation of additional devices (e.g. resistors, voltage generators or

Table 13
Power bundle results for (a) bundle 1 and (b) bundle 2

Electrochemistry	Part number	Discharge current (A)	Energy (Wh)	Nominal voltage (V)	x (energy ratio)	y (voltage ratio)	z (current ratio)	n (number of batteries)	s (series)	w (parallel)	M (kg)	$\hat{V}_j$ (L)	Number of cycles (not including recharge cycles)	Lifetime (h)	Specific energy (Wh kg^{-1})	Energy density (Wh L^{-1})
Bundle 1																
Manganese lithium	ML414S	5.00E − 06	0.004	3.0	105.9	5.7	88400.00	530400.00	6.00	88400.00	42.432	13.4370	5.01E + 03	1.44E + 06	45.00	142.10
	ML421S	3.00E − 06	0.007	3.0	55.3	5.7	147333.33	884004.00	6.00	147334.00	97.240	33.593	1.60E + 04	4.59E + 06	62.73	181.58
	HHR60AAAH	1.00E − 01	0.600	1.2	0.6	14.2	4.42	75.00	15.00	5.00	0.900	0.289	118.005	1.69E + 04	50.00	155.71
	HHR70AAAJ	1.44E − 01	0.864	1.2	0.4	14.2	3.07	60.00	15.00	4.00	0.780	0.231	135.941	1.95E + 04	66.46	224.23
Nickel metal hydride	NH50-D	5.00E − 01	3.000	1.2	0.1	14.2	0.88	15.00	15.00	1.00	1.095	0.847	118.005	1.69E + 04	41.10	53.10
	NH35-C	5.00E − 01	3.000	1.2	0.1	14.2	0.88	15.00	15.00	1.00	0.900	0.404	118.005	1.69E + 04	50.00	111.29
	NH12-AAA	1.70E − 01	1.020	1.2	0.4	14.2	2.60	45.00	15.00	3.00	0.540	0.173	120.365	1.73E + 04	85.00	264.71
	NH15-AA	4.60E − 01	2.760	1.2	0.1	14.2	0.96	15.00	15.00	1.00	0.405	0.125	108.564	1.56E + 04	102.22	330.97
	NH22-9V	3.00E − 01	0.180	1.2	2.1	14.2	14.73	225.00	15.00	15.00	9.225	4.887	106.204	1.52E + 04	4.39	8.29
Lithium ion	SP180AAKH	1.50E − 01	0.900	1.2	0.4	14.2	2.95	45.00	15.00	3.00	0.585	0.150	1.06E + 02	1.52E + 04	69.23	269.63
	SP230AAKH	3.60E − 01	2.160	1.2	0.1	14.2	1.23	30.00	15.00	2.00	0.840	0.238	1.70E + 02	2.44E + 04	77.14	272.78
	SP230AAKH	4.60E − 01	2.760	1.2	0.1	14.2	0.96	15.00	15.00	1.00	0.450	0.115	1.09E + 02	3.11E + 04	92.00	358.59
	CGR17500	1.56E − 01	2.988	3.6	0.1	4.7	2.83	15.00	5.00	3.00	0.375	0.167	1.18E + 02	1.68E + 04	119.52	268.56
	CGR18650HG	3.40E − 01	6.660	3.7	0.1	4.6	1.30	10.00	5.00	2.00	0.420	0.175	1.75E + 02	2.50E + 04	158.57	381.18
	UBC641730/PCM	1.90E − 01	0.740	3.7	0.5	4.6	2.33	15.00	5.00	3.00	0.068	0.058	2.91E + 01	2.50E + 03	164.44	192.20
	UBP383450/PCM	5.90E − 01	2.220	3.7	0.2	4.6	0.75	5.00	5.00	1.00	0.069	0.043	2.91E + 01	4.17E + 03	160.87	259.54
	UBC422030/PCM	1.40E − 01	0.555	3.7	0.7	4.6	3.16	20.00	5.00	4.00	0.080	0.061	2.91E + 01	2.50E + 04	138.75	181.39
	ICP383450G	1.40E − 01	2.590	3.7	0.1	4.6	3.16	20.00	5.00	4.00	0.290	0.132	1.36E + 02	1.95E + 04	178.62	393.01
	ICP383450G	1.44E − 01	2.664	3.7	0.1	4.6	3.07	20.00	5.00	4.00	0.290	0.130	1.40E + 02	2.00E + 04	183.72	410.70
	CGA523450A	9.00E − 01	3.276	3.6	0.1	4.7	0.49	5.00	5.00	1.00	0.098	0.045	4.30E + 01	6.16E + 03	168.00	367.06
	CGA523436	6.80E − 01	2.520	3.6	0.2	4.7	0.65	5.00	5.00	1.00	0.073	0.032	3.30E + 01	4.74E + 03	173.79	395.93
Nickel cadmium	P-11AAH	2.40E − 02	0.144	1.2	2.6	14.2	18.42	285.00	15.00	19.00	1.853	0.824	1.08E + 02	1.54E + 04	22.15	49.83
	P-18N	3.80E − 02	0.228	1.2	1.7	14.2	11.63	180.00	15.00	12.00	1.440	0.611	1.08E + 02	1.54E + 04	28.50	67.20
	SP30AA2/3MC	1.50E + 00	0.360	1.2	1.1	14.2	0.29	15.00	15.00	1.00	0.165	0.068	1.42E + 01	2.03E + 03	32.73	79.76
	SP28AAAMC	1.40E + 400	0.336	1.2	1.1	14.2	0.32	15.00	15.00	1.00	0.135	0.052	1.32E + 01	1.89E + 03	37.33	96.98

Electrochemistry	Part number	Discharge current (A)	Energy (Wh)	Nominal voltage (V)	x	y	z	n	s	w	M (kg)	Area (cm^2)	Number of cycles (not including recharge cycles)	Lifetime (h)	Energy density (Wh cm^{-2})
Bundle 2															
Lithium-free thin-film batter	–	5.00E − 03	7.2E − 01	3.60	0.41	4.72	12.00	60	5	12	–	60	1.5E + 02	21176.47	7.20E − 01

Table 14
Comparison of Approaches 1, 2, and 3 with and without CMOS op-amps and novel voltage generator technologies [28–31]

Results-exclusion of op-amp technology (inclusion of op-amp technology)					
Approach	Battery type(s)	Number of batteries	Total mass (kg)	Total volume (L)	Lifetime (h)
1	Lithium polymer battery—prismatic	15 (1)	0.068 (0.014)	0.058 (0.012)	2.4E03 (8.13E02)
2	Lithium-free thin-film prismatic lithium ion	8 (4)	0.032 (0.014)	0.028 (0.012)	8.9E03 (8.9E03) (mW range), 979 (979) (mW range), 164 (233) (W range)
3	Lithium-free thin-film prismatic lithium polymer	65 (61)	0.073 (0.015)	0.032 (0.006)	2.1E04 (9.5E02) (bundle 1), 4.7E03 (2.1E04) (bundle 2)

Commercial CMOS op-amp, and high-voltage generator characteristics					
Manufacturer	Part number	Supply voltage range V_{cc} (V)	Open loop gain A (dB)	Operational temperature (C)	Areal footprint (cm^2)
Texas Instruments [29]	OPA725	4–12	100	−40 to 125	0.09
Texas Instruments [29]	OPA2725	4–12	100	−40 to 125	0.16
Seiko Instruments [30]	S-89110A/89120A	1.8–5.5	80	−40 to 85	0.04
University of Michigan [31]	High-voltage generator	Maximum voltage achieved >200 V	>300	–	0.16

op-amps) to accommodate for voltage gains above nominal voltages of batteries in the database. Instead, system voltages greater than nominal voltages of the database batteries, were accommodated by placing batteries in series. In this section of the document, we briefly examine implementation of op-amp or voltage generator technology to achieve voltages substantially higher than the nominal battery voltage values. We explore use of op-amps because assembling separate transistors, resistors, and capacitors on a circuit board is an expensive and wasteful procedure, while use of integrated-circuit (IC) amplifiers is preferential because they are versatile, compact, and inexpensive. Op-amps are a collection of circuit elements used to increase voltage, current, or power within a system, that can be single stage (consisting of a single transistor) or multistage (more than one stage); e.g. voltage follower, noninverting, inverting, summing, and current-to-voltage converter. We have selected noninverting op-amps [29,30] or voltage generators [31], to achieve voltage gain for the three approaches providing voltage ratio values (y) greater than 1. Table 14 details some typical characteristics of commercial CMOS op-amp devices along with a novel voltage generator technology demonstrated by Udeshi [31]. Table 14 summarizes results for all three approaches for cases where voltage generators [31] are used and not used. The mass and volume of the voltage generator(s) are not included in the mass and volume calculations.

6. Discussion

Table 14 summarizes the results from each approach. The advantages of using these approaches are that it is a systematic method for the assembly of voltage and discharge current data that readily lends itself to the application of conditionality statements and step-wise selection techniques that deliver an optimal solution to a general MEMS power problem.

All of these approaches produce mass and volume values that surpass the target values, 0.0043 kg and 0.00145 cm^3. The specific energy and energy density values calculated for each approach assume theoretical capacity of active materials. In fact, the actual energy available from a real battery under practical, but close to optimal discharge conditions is only about 25–35% of the theoretical energy of the active materials [17], because battery manufactures must include electrolyte, packaging, and additives to enhance conductivity in the calculation of the specific energy and energy density of their products.

Approach 2 provided the best results of mass (0.032 kg) and volume (0.028 L) among the three approaches. Specifically, use of Approach 2 results in masses 47.1 and 43.8% and volumes 48.3 and 87.5% of Approaches 1 and 3, respectively. In general, Approaches 2 and 3 provided the best battery lifetime results; both systems produced lifetimes in excess of 2E3 h. Approach 3 required the most batteries (4.3 and 8.1 times Approaches 1 and 2), which increases the probability of system failure and fabrication complexity.

Approach 1 is appropriate for systems having relatively low and constant current drain rates and nominal voltage values, small to moderate cycle times, and sufficient time for slow to moderate (4–5 h) charging time. Also this approach provides additional benefits of a less design and fabrication complexity since only one electrochemistry is used. However, additional capacity or battery lifetime achieved from the additional cells for accommodation of fluctuations in discharge current and voltage; can potentially result in heavy and large systems. Extensive power management systems could be necessary to adequately manage the different discharge current and voltage requirements of the system.

Approach 2 capitalizes on the variability of battery performance based on shape and fabrication, to reduce mass and volume power requirements. It, unsurprisingly, resulted in the smallest mass and volume values (0.032 kg and 0.028 L, respectively) for the systems studied. Also, this strategy allows power size, shape, and manufacturability to be considered for optimal battery lifetime and system mass and volume constraints, as demonstrated with the implementation of thin-film battery technology for the micro-power range, and thin prismatic cells for both the mW and W power ranges.

Despite the many advantages of Approach 2, it is not suitable for all systems, for example, power system fabrication complexity, could be increased as each battery type could require a different fabrication technique. This approach also generally does not account for battery lifetime; in the case studied here, it provided the shortest battery lifetime predictions for the mW and W power ranges (979 and 164 h, respectively, excluding the μW power range). Also, use of different battery electrochemistries requires different charging programming for each electrochemistry used.

Approach 3 provided the worse values for mass (0.073 kg) of all approaches, however, provided a volume very close to Approach 2 (∼1.14 times). However, use of smaller stand-alone power systems is a safe guard against complete system failure that can occur when only one power system is used. This approach allows an additional degree of freedom, in that instead of a maximum of only three electrochemistries being an option for the power system, the maximum number of electrochemistries that can be implemented is equal to the number of subdevices and/or power bundles.

It is obvious from comparison of results listed in Table 14 that use of voltage generator or noninverting op-amp technology can certainly reduce the mass and volume of a power system in cases where power ranges are low to moderate, while voltage values are in excess of 3.7 V. However, mass, volume and surface area of op-amps and/or voltage generators must also be weighed in power system design, along with required power and discharge current for operation. Also, op-amp performance as a function of temperature is important as drift (inaccurate voltage gain values due to temperature variation) becomes more probable at high-operation temperature temperatures.

Use of multiple battery power sources can increase the probability of system failure due to the increase in the number of fabrication steps and power subdevices. In this case study, 65 batteries are required; other workers have also implemented multiple thin-film batteries in series and parallel [10]. Also, this approach is limited by additional mass, volume, and areal footprint that may be necessary for individual power supplies for each component along with additional manufacturing time.

In this case study, user prescribed power bundle configurations were used based on packaging and continuity of fluid flow constraints, which precluded detailed consideration of locations of power bundle sites. This has a profound impact on results obtained here, as the WIMS–EMT consists of 10 subdevices, which lends itself to numerous permutations that were not examined here.

7. Conclusions

Through this analysis of the WIMS–EMT, we have demonstrated that the solution to power supply problem will most likely be a nonlinear optimization problem, subject to both linear and nonlinear constraints and that the most efficient power design will most likely be a hybrid power system based on the superior performance of both hybrid systems from Approaches 2 and 3. Approach 2 provided the best results of mass (0.032 kg) and volume (0.028 L) among the three strategies. Specifically, use of Approach 2 results in masses 47.1 and 43.8% and volumes 48.3 and 87.5% of Approaches 1 and 3, respectively. In general, Approaches 1 and 3 provided the best battery lifetime results wherein both predicted lifetimes in excess of 2E3 h. Approach 3 required the most batteries (4.3 and 8.1 times Approaches 1 and 2), which increases the probability of system failure and fabrication complexity.

Diversity of battery types within the database, i.e. high-energy density and high-power density materials is imperative for effective power supply design. The availability of battery performance data, such as cell capacity as a function of discharge rate is crucial, as calculation of energy and current factors (x and y) depends on it. Specifically, relationships between discharge rate and capacity can prevent the elimination of batteries unnecessarily, such as when only one capacity at one discharge rate is provided. Results from the implementation of this algorithm are only as reliable as the source of the battery characteristics: the battery database. Incomplete data, i.e. little to no data on capacity of battery at various discharge rates, can result elimination of viable power solutions early in the optimization process.

8. Future work

Our method of predicting battery life was clearly approximate. By assuming all cycles occur continuously, battery recovery, i.e. recovery of battery voltage that occurs when a battery stands idle after a discharge, was not taken into account. Also, potential battery self-discharge was not taken into account. Reduction in battery capacity with subsequent discharge cycles was similarly not accounted for in the present work. Collectively, these assumptions could result in significant overestimates of battery lifetime, and will be investigated as part of future work.

Experimental verification of code predictions will also follow. Other possible selection criteria not investigated in this document, but of importance, are power system cost, number of manufacturing steps, complexity, probability of failure due to system complexity, and temperature. Of these, we will next focus on the probability of failure due to system complexity,

along with incorporation of some CMOS op-amp technologies to accommodate large voltage fluxes in many MEMS devices. Also, other means of grouping based on power bundle location, wherein, varying the number of devices within a set number of bundle locations will be investigated. Lastly, work in establishing an effective method for prediction of battery capacity as a function of electrochemical reaction rates will be pursued. Ultimately, we aim, as part of future work, to implement our verified approaches, conditionality statements, and selection techniques within a user-friendly code.

References

[1] WIS ERC Annual Report 2003. University of Michigan College of Engineering, NSF engineering Research Center for Wireless Integrated MicroSystems, available at: http://www.wimserc.

[2] P.J.M. Havinga, G.J.M. Smit, Design techniques for low power systems, J. Syst. Architecture 64 (1) (2000) 1–21.

[3] M. Engels, Technology challenges in the development of wireless personal area networks, Wireless Pers. Commun. 22 (2002) 319–329.

[4] W. Mangione-Smith, Technical challenges for designing personal digital assistants, Design Autom. Embedded Syst. 4 (1999) 23–29.

[5] H. Partovi, K. Soumyanath, T. Sakurai, C.T. Chuang, S.L. Lu, V. De, Challenges for low-power and high-performance chips - A D & Troundtable, IEEE Design Test Comput. 15 (3) (1998) 119–124.

[6] Y. Zhang, H.H. Chen, J.B. Kuo, 0.8 V CMOS adiabatic differential switch logic circuit using bootstrap technique for low-voltage low-power VLSI, Electron. Lett. 38 (24) (2002) 1497–1499.

[7] R.G. Carvajal, J. Galan, J. Ramirez-Angulo, A. Torralba, Low-power low-voltage differential class-AB OTAs for SC circuits, Electron. Lett. 38 (22) (2002) 1304–1305.

[8] G. Gramegna, P. O'Connor, P. Rehak, S. Hart, CMOS preamplifier for low-capacitance detectors, Nuclear Instrum. Methods Phys. Res. A 390 (1997) 241–250.

[9] J.B. Bates, N.J. Dudney, D.C. Lubben, G.R. Gruzalski, B.S. Kwak, X. Yu, Thin-film rechargeable lithium batteries, J. Power Sources 54 (1995) 58–62.

[10] S.D. Jones, J.R. Akridge, Development and performance of a rechargeable thin-film solid-state microbattery, J. Power Sources 54 (1995) 63–67.

[11] D. Singh, R. Houriet, R. Giovannini, H. Hofmann, V. Craciun, R.K. Singh, Challenges in making of thin films for $Li_xMn_yO_3$ rechargeable lithium batteries for MEMS, J. Power Sources 97–98 (2001) 826–831.

[12] N. Takami, M. Sekino, T. Ohsaki, M. Kanda, M. Yamamoto, New thin lithium-ion batteries using a liquid electrolyte with thermal stability, J. Power Sources 97–98 (2001) 677–680.

[13] B. Huang, C.C. Cook, S. Mui, P.P. Soo, D.H. Staelin, A.M. Mayes, D.R. Sadoway, High energy density, thin-film, rechargeable lithium batteries for marine field operations, J. Power Sources 97–98 (2001) 674–676.

[14] S.V. Kosonocky, A.J. Bhavnagarwala, K. chin, G.D. Gristede, A.-M. Haen, W. Hwang, M.B. Ketchen, S. Kim, D.R. Knebel, K.W. Warren, V. Zyuban, Low-power circuits and technology for wireless digital systems, IBM J. Res. Dev. 47 (2/3) (2003) 283–298.

[15] S. Mutoh, T. Douseki, Y. Matsuya, T. Aoki, S. Shigematsu, J. Yamada, 1-V power supply high-speed digital circuit technology with multithreshold-voltage CMOS, IEEE J. Solid State Circuits 30 (1995) 847–854.

[16] K. Nii, H. Makino, Y. Tujihashi, C. Morisha, Y. Hayakaw, H. Nunogami, T. Arakawa, H. Hamano, A low power SRAM using auto-backgate-controlled MT-CMOS, in: Proceedings IEEE/ACM International Symposium on Low Power Electronic Devices, 1998, pp. 293–298.

[17] D. Linden, T.B. Reddy, Handbook of Batteries. 3rd ed. McGraw-Hill Companies, Inc., New York2002, (1.3-1.17, 7.10-7.11, 22.12-22.13).

[18] Y.J. Park, K.S. Park, J.G. Kim, M.K. Kim, H.G. Kim, H.T. Chung, Characterization of tin oxide/$LiMn_2O_4$ thin-film cell, J. Power Sources 88 (2000) 250–254.

[19] http://duracell.com, April 25, 2004.

[20] B.Y. Liaw, E.P. Roth, R.G. Jungst, G. Nagasubramanian, H.L. Case, D.H. Doughty, Correlation of Arrhenius behaviors in power and capacity fades with cell impedance and heat generation in cylindrical lithium-ion cells, J. Power Sources 119–121 (2003) 874–886.

[21] L.P. Jarvis, T.B. Atwater, P.J. Cygan, Fuel cell/electrochemical capacitor hybrid for intermittent high power applications, J. Power Sources 79 (1) (1999) 60–63.

[22] P.B. Jones, J.B. Lakeman, G.O. Mepsted, J.M. Moore, A hybrid power source for pulse power applications, J. Power Sources 80 (1999) 242–247.

[23] M.A. Elhadidy, S.M. Shaahid, Optimal sizing of battery storage for hybrid (wind + diesel) power systems, Renewable Energy 18 (1) (1999) 77–86.

[24] A. Mason, N. Yazdi, A.V. Chavan, K. Najafi, K.D. Wise, A generic multielement microsystem for portable wireless applications, Proc. IEEE 86 (8) (1998) 1733–1746.

[25] R.G. Carvajal, A. Torralba, J. Tombs, F. Munoz, J. Ramirez-Angulo, Low voltage class AB output stage for CMOS op-amps using multiple input floating gate transistors, Analog Integrated Circuits Signal Process. 36 (2003) 245–249.

[26] A. Torralba, R.G. Carvajal, J. Ramirez-Angulo, J. Tombs, R. Munoz, J.A. Galan, Class AB output stages for low voltage CMOS op-amps with accurate quiescent current control by means of dynamic biasing, Analog Integrated Circuits Signal Process. 36 (2003) 67–77.

[27] B.J. Neudecker, N.J. Dudney, J.B. Bates, Lithium-free thin-film battery with in situ plated Li anode, J. Electrochem. Soc. 147 (2) (2000) 517–523.

[29] http://focus.ti.com/docs/prod/folders/print/opa725.html# technicaldocuments.

[30] http://www.sii.ic.com/en/.

[31] K. Udeshi, Y.B. Gianchandani, A transistorless micro mechanical high voltage generator using a DC-powered self-oscillating relay, in: Proceedings of the Solid-state Sensor, Actuator, and Microsystems Workshop, June 6–10, 2004.